ESO Phase 3 Data Release Description

Data Collection	VIDEO_ES1
Release Number	1
Data Provider	Matt Jarvis
Date	04.04.2014

Abstract

VIDEO is a deep near-infrared survey which targets ~12 square degrees over the ELAIS-S1, XMMLSS, and ECDFS extragalactic fields. This document describes the first release of individual VISTA tiles in the ELAIS-S1 field from observing run IDs 179.A-2006(B,C,D,E).

Overview of Observations

We release the individual tiles and associated sources lists from the VISTA Deep Extragalactic Observations (VIDEO) Survey. We release single-OB tiles in Z, H and Ks bands in the VIDEO-ES1 field along with the associated source lists (see Fig. 1) taken between 06/10/2010 - 15/11/2011. Coverage over the full 3.0 square degrees of the ES1 field will be provided in future releases. This release of the VIDEO-ES1 field follows the same steps as described in the VIDEO survey paper for the VIDEO-XMM release (Jarvis et al. 2013).

Release Content

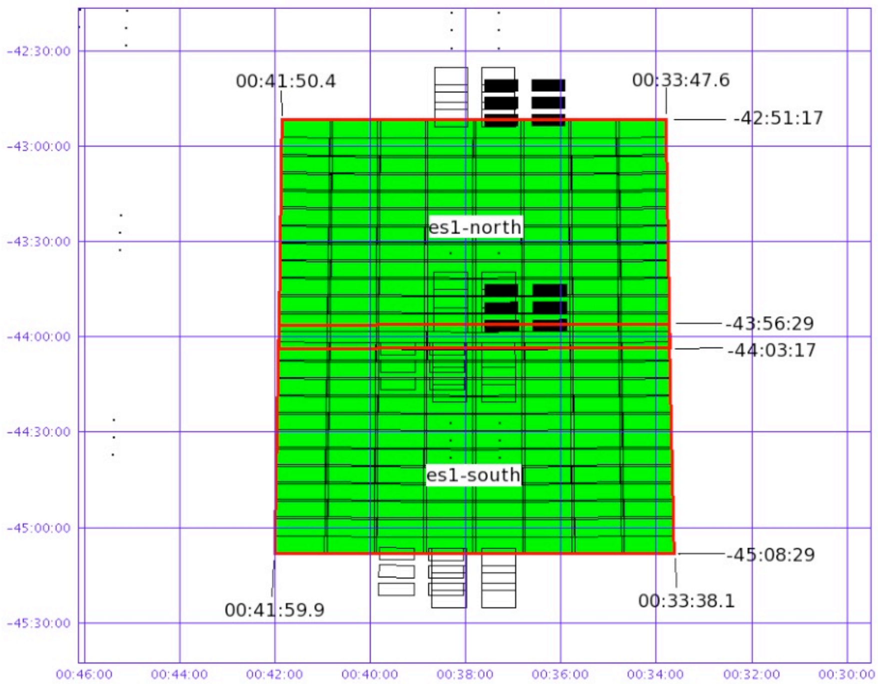

Figure 1. The coordinates of the VIDEO-ES1 field. This release comprises data over the ES1-North and ES1-South fields.

Table 1. Single-OB tiles released. Note that two observing strategies for the Z-band data in the VIDEO-ES1N field were used. These are denoted at Z(1) and Z(2). These can be differentiated between within the image headers by checking the EXPTIME keywords, which corresponds to the *Integration/pixel* in the table below. One early observation in Z band was carried out with an integration time of 870s, again this is denoted by the EXPTIME keyword in the header and is given as Z(3) in the table. We note that in a few cases Z(1) is not 2970 due to the non-completion of OBs. One observation in ES1S in the Ks band was carried out with a shorter integration time (denoted Ks(2)).

Field	Filter	*Integration/tile*	*Integration/pixel*	*Number of Tiles*
VIDEO-ES1N	Z(1)	2970 sec	990 sec	13
VIDEO-ES1N	Z(2)	3000 sec	1000 sec	14
VIDEO-ES1N	Z(3)	2610 sec	870 sec	1
VIDEO-ES1N	H	2520 sec	840 sec	5
VIDEO-ES1N	Ks	2520 sec	840 sec	24
VIDEO-ES1S	Z	2700 sec	900 sec	18
VIDEO-ES1S	Ks(1)	2520 sec	840 sec	43
VIDEO-ES1S	Ks(2)	2160 sec	720 sec	1

Release Notes

Data Reduction and Calibration

The reduction of this data was carried out at the Cambridge Astronomy Survey Unit as part of the VISTA Data Flow System described by Irwin et al. (2004). Full details of the reduction, calibration based on 2MASS and the source list generation for this release can be found at http://casu.ast.cam.ac.uk/surveys-projects/vista/technical/data-processing. The tiles have been processed continually from the start of the VIDEO survey, as such the version of the pipeline used for the reduction is given by the PROCSOFT keyword in the headers. In future releases these will all be updated using the latest version of the pipeline. Here we provide a brief summary of the steps implemented in generating the tiles for the VIDEO survey.

· **Reset correction:** Reset frames are taken for each exposure and are subtracted in the data acquisition system.

· **Dark correction:** the dark current is estimated from a series of exposures taken with a dark filter inserted and then subtracted.

· **Linearity correction:** the VISTA detectors do not have a linear response. To estimate the non-linearity of each detector we need information on the readout timing, the exposure time and the reset image timing (this is because there is no shutter on the camera and in double-correlated sampling mode, the default, the reset frame is subtracted prior to writing images to disk).

· **Flat field correction:** dividing by a mean twilight flatfield image removes the small scale QE variations in the detector as well as the large scale vignetting profile of the camera. We also use the global flatfield properties of each detector to gain-normalise each detector to a common (median) system.

· **Sky background correction:** this removes the large scale spatial background emission that comes from the atmosphere as well as several remaining additive effects. The 2d background map is estimated using several different algorithms that combine the science images themselves with masking of bright objects. Subsequent releases will use a mask based on the deep stacked images for more accurate sky subtraction

· **Destripe:** the readout electronics for the VISTA detectors introduce a low-level horizontal stripe pattern into the background. This is removed as a processing step.

· **Jitter stacking:** At this point in the reduction the jitter series is shifted and combined to form a single image stack, using positions of detected objects on all the detectors to compute the shifts. This allows bad pixel regions in one exposure to be rejected in favour of good pixels in other exposures.

· **Source list generation:** information on astronomical objects on the individual tiles are extracted at this point. The parameters include positions, fluxes, and shape descriptors which are combined to generate object morphological classifications and form the basis for calibration and QC information.

· **Astrometric and photometric calibration:** objects in the source lists are matched to their counterparts in the 2MASS point source catalogue. Because 2MASS has such a high degree of internal consistency it is possible to calibrate the world coordinate system of VISTA images to better than 50 milli-arcseconds. The 2MASS magnitudes are also used in conjunction with colour equations (see below) to provide photometric zeropoints to an accuracy of 1-2% (depending upon the wave band).

· **Tiling:** the overlap areas in VISTA pawprints needed to form a contiguous tile are large, so the pawprints are combined into tiles. Once this is done the source extraction step is repeated.

Colour equations based on 2MASS photometry (See Hodgkin et al. 2009)

$Z_{VIDEO} = J_{2MASS}+1.025(J_{2MASS}-H_{2MASS})$
$Y_{VIDEO} = J_{2MASS}+0.610(J_{2MASS}-H_{2MASS})$
$J_{VIDEO} = J_{2MASS}-0.077(J_{2MASS}-H_{2MASS})$
$H_{VIDEO} = H_{2MASS}+0.032(J_{2MASS}H_{2MASS})$
$Ks_{VIDEO} = Ks_{2MASS}+0.01(J_{2MASS}-Ks_{2MASS})$

Data Quality

- Astrometric checks have been carried out by comparing with the 2MASS stars within the tiled fields. No systematic offsets are found and the rms scatter is found to be ~0.25 arcsec.
- The zero point is uniform across the tile to within the quoted uncertainty (<0.01 mag).
- Photometry has also been checked against unresolved 2MASS sources within the VIDEO field. We find very good agreement between 2MASS and VIDEO after applying the colour equations to move from the 2MASS system to the VIDEO photometric system.

Known issues

Regions of bad pixels in Detector 1 and time varying quantum efficiency in detector 16 renders these detectors the most problematic. The regions of poorer noise statistics are evident in the confidence images.

For the ELAIS-S1-North tile the central position is shifted slightly between for some observations (e.g. H-band compared to Z and Ks). The tile centre is given by the TL_RA and TL_DEC keywords in the header information and these provide the centre of the given tile.

Previous Releases

This is the first VIDEO release for the VIDEO-ES1 field. Previous VIDEO releases contained data over the VIDEO-XMM field.

Data Format

Files Types

We release individual tile images and their associated confidence images, which have the same filename but with "_conf" and the corresponding source lists have a "_cat" appended. These are a combination of reductions using versions 1.1 and1.2 of the reduction pipeline, as this was updated during the period of observations. Subsequent releases will be reprocessed through the latest single pipeline.

The single-tile images, confidence maps and source lists have the following naming convention:
v$DATE$_OBS_NUMBER_st_tl.fits.fz
v$DATE$_OBS_NUMBER_st_tl_conf.fits.fz
v$DATE$_OBS_NUMBER_st_tl_cat.fits

for the tiled image, the confidence image and the source list respectively. OBS_NUMBER refers to the final observation number for the individual paw-prints which contribute to the tile.

The individual-tile source list format was derived from similar APM/SuperCOSMOS/INTWFC/CIRSI analysis which produced 32 4-byte parameters per detected object. This was first enhanced for WFCAM to an 80 4-byte parameter set to include extra parameters for flux estimation and error estimates, and this has now been further refined for the VIRCAM catalogues. The following table covers the VIRCAM standard and further processing pipeline output source lists, where for simplicity all derived parameters are stored as floating point numbers even though some of them are more naturally integers. See http://casu.ast.cam.ac.uk/surveys-projects/vista/technical/catalogue-generation for more information.

Table 2. Complete list of supplied columns for the sources lists released with the individual tiles.

No	Name	Column Description
1	Seq No.	Running number for ease of reference, in strict order of image detections
2	Isophotal flux	Standard definition of summed flux within detection isophote, apart from detection filter is used to define pixel connectivity and hence which pixels to include. This helps to reduce edge effects for all isophotally derived parameters.
3	X coord	Intensity–weighted isophotal centre–of–gravity in X
4	Error in X	Estimate of centroid error
5	Y coord	Intensity–weighted isophotal centre–of–gravity in Y
6	Error in Y	Estimate of centroid error
7	Gaussian sigma	These are derived from the three general intensity–weighted second moments
8	Ellipticity	The equivalence between them and a generalised elliptical Gaussian
9	Position angle	Position angle of the isophote
10-17	Areal profile 1-8	Number of pixels above a series of threshold levels relative to local sky. Levels are set at T, 2T, 4T, 8T . . . 128T where T is the threshold.

		These can be thought of as a radial profile. Note that for now, deblended, i.e. overlapping images, only the first areal profile is computed and the rest are set to −1 flagging the difficulty of computing accurate profiles for blended images this parameter is used to flag the start of the sequence of the deblended components by setting the first in the sequence to 0.
18	Peak height	In counts relative to local value of sky - also zeroth order aperture flux
19	Error in pkht	Error in Peak Height
20-45	Aperture flux 1-13 and error on aperture flux 1-13	These are a series of different radii soft-edged apertures designed to adequately sample the curve-of-growth of the majority of images and to provide fixed-sized aperture fluxes for all images. The scale size for these apertures is selected by defining a scale radius _<FWHM> for site+instrument. In the case of VIRCAM this "core" radius (rcore) has been fixed at 1.0 arcsec for convenience in inter-comparison with other datasets. A 1.0 arcsec radius is equivalent to 3.0 pixels for normal data. In 0.8 arcsec seeing an rcore-radius aperture contains roughly 75% of the total flux of stellar images. The aperture fluxes are sky-corrected integrals (summations) with a soft-edge (i.e. pro-rata flux division for boundary pixels). However, for overlapping images they are more subtle than this since they are in practice simultaneously fitted top-hat functions, to minimise the effects of crowding. Images external to the blend are also flagged and not included in the large radius summations. Starting with parameter 20 the radii are: 1/2× rcore, 1/sqrt(2)× rcore, rcore, sqrt(2)× rcore, 2× rcore, 2sqrt(2)× rcore, 4× rcore, 5× rcore, 6× rcore, 7× rcore, 8× rcore, 10× rcore, 12× rcore We recommend using Aperture flux 3 if a single number is required to represent the flux for ALL images - this aperture has a radius of rcore = 1 arcsec.
46	Petrosian radius	Petrosian radius as defined in Yasuda et al. 2001 AJ 112 1104
47	Kron radius	Kron radiusas defined in Bertin and Arnouts 1996 A&A Supp 117 393
48	Hall radius	Hall image scale radius eg. Hall & Mackay 1984 MNRAS 210 979
49	Petrosian flux	Petrosian flux within circular aperture to k x rp with k=2
50	Error in flux	Error on Petrosian flux
51	Kron flux	Flux within circular aperture to k x rk with k=2
52	Error in flux	Error on Kron flux
53	Hall flux	Flux within circular aperture to k x rh with k=5; alternative total flux
54	Error in flux	Error on Hall flux
55	Error bit flag	Bit pattern listing various processing error flags initially set to the no. of bad pixels within aperture of radius "rcore"- note this can be fractional due to soft-edged apertures
56	Sky level	Local interpolated sky level from background tracker
57	Sky rms	Local estimate of variation in sky level around image
58	Av conf	Average confidence level within default rcore aperture useful for spotting spurious outliers in various parameter selection spaces
		The following are accreted after standard catalog generation
59	RA	Right Ascension in radians (J2000)
60	Dec	Declination in radians(J2000)
61	Classification	Flag indicating most probable morphological classification: eg. −1 stellar, +1 non−stellar, 0 noise, −2 borderline stellar (Saturated images can be flagged by comparing the peak height + local sky with the SATURATE keyword in the header.)
62	Statistic	An equivalent N(0,1) measure of how stellar−like an image is, used in deriving parameter 61 in a 'necessary but not sufficient' sense. Derived mainly from the curve-of-growth of flux using the well-defined

		stellar locus as a function of magnitude as a benchmark (see Irwin et al. 1994 SPIE 5493 411 for more details).
63	MJDoff	The number of minutes to be added to MJD_DAY in order to get the MJD of a given object. Hence for the *i*th object: MJDi = MJD_DAY + MJDoffi /1440.0
64	Blank	Blank
65	Blank	Blank
66	Blank	Blank
67	Blank	Blank
68	Blank	Blank
69	Blank	Blank
70	Blank	Blank
71	Blank	Blank
72	Blank	Blank
73	Blank	Blank
74	Blank	Blank
75	Blank	Blank
76	Blank	Blank
77	Blank	Blank
78	Blank	Blank
79	Blank	Blank
80	Blank	Blank

Acknowledgements

The VIDEO Survey is described in Jarvis et al. 2013, MNRAS, 428, 1281 and any publications using the VIDEO data should reference this article.

Please use the following statement in your articles when using these data:
Based on data products from observations made with ESO Telescopes at the La Silla Paranal Observatory under programme ID 179.A-2006.

References

Hodgkin S.T., et al., 2009, 394, 675
Irwin M.J., et al., 2004, SPIE, 5493, 411
Jarvis M.J., et al., 2013, MNRAS, 428, 1281